Neutron emission in ^{19}F-induced reactions

Jaimin Acharya, S. Mukherjee, A. Chatterjee, N. L. Singh, K. Ramachandran, P. C. Rout, K. Mahata, Vishal Desai, E. T. Mirgule, S. V. Suryanarayana, B. K. Nayak, A. Saxena, and G. F. Steyn

Neutron emission in ^{19}F induced reactions

Jaimin Acharya, S. Mukherjee [*], A. Chatterjee, N.L. Singh

Department of Physics, The M.S. University of Baroda, Vadodara - 390002, India

K. Ramachandran, P.C. Raut, K. Mahata, Vishal Desai, E.T. Mirgule, S.V. Suryanarayana,

B.K. Nayak and A. Saxena

Nuclear Physics Division, Bhabha Atomic Research Centre, Mumbai - 400085, India

G.F. Steyn

iThemba LABS, Somerset West, South Africa

Abstract

We have measured neutron emission spectra for ^{19}F induced reactions on ^{181}Ta, ^{89}Y and ^{51}V at beam energies 130, 140, 145 and 150 MeV. Measurements were made using liquid scintillator detectors at eight angles in the range of 25°-143°usingtime-of-flight and pulse-shape discrimination. A comparison has been made with ALICE2014 and PACE4 calculations to understand the role of incomplete fusion and pre-equilibrium effects. Global predictions with ALICE2014 without parameter adjustment gives a fair agreement with the measured data.

(*) Corresponding Author: sk.mukherjee-phy@msubaroda.ac.in

I. Introduction

Many attempts have been made to understand the pre-equilibrium process in terms of nucleon-nucleon interactions within the target nucleus [1-6]. In the last few decades, several quantum mechanical theories have been proposed which can provide a way of calculating cross-sections of pre-equilibrium processes without the uncertainties of semi-classical approximations. With increasing bombarding energy especially at forward angles and higher emission energies, pre-equilibrium effects can be pronounced and in some cases it could be the dominant reaction mechanism.

From a nuclear data standpoint, it is not sufficient to have a theory that will fit the available experimental data with parameter values adjusted from case to case. Rather a theory with a global perspective that can be used with some confidence to predict cross-section of reactions that have not yet been measured or are difficult or not possible to measure is needed. Several computer codes are available for quantum mechanical theories so it is desirable to test their ability to calculate the required cross sections. More importantly we want to know how accurately they are able to calculate without arbitrary variation of parameters.

During the past few decades the Monte Carlo pre-equilibrium model has been developed that provides certain advantages for use in modelling nuclear reactions and generating evaluated ENDF (Evaluated Nuclear Data File) databases. The initial formulation by Blann [7] was subsequently expanded to include the treatment of ejectile angular and energy distribution in a new pre-compound model [8]. Another pre-compound Monte Carlo model was introduced to take care of the treatment of the cluster induced reactions [9]. This approach is valuable because of its ability to accurately model a comprehensive variety of nuclear reaction mechanisms that occur for the projectiles with incident energies up to a few hundred MeV. Presently two implementations of this approach exist: Blann's Monte Carlo version of ALICE [7-9]; and Chadwick's DDHMS (Double Differential Hybrid Monte Carlo Simulation) [8-12] code. In this paper we have tested the accuracy and ability of the latest version of Blann's code, ALICE2014 to predict neutron emission cross-sections in heavy ion reactions [13].

In order to understand the role of pre-equilibrium emission, we have also compared our results with the statistical model code PACE4 (Projection Angular Momentum Coupled Evaporation) [14] commonly used in calculating spectra of particles in heavy-ion induced

reactions. Since the PACE4 code does not take into account the pre-equilibrium and the breakup processes, such a comparison is indicative of the pre-equilibrium components. Deviations between ALICE2014 and PACE4 in regions of the spectra where pre-equilibrium effects are not expected to contribute significantly are indicative of other assumptions for a similar set of parameters used in the two codes. In addition to pre-equilibrium effects, neutron emission at low energies and forward angles also include a contribution from breakup. The ALICE2014 calculations include breakup by using the Fermi statistics breakup model [15]. In this model, the densities of excited states are taken into account, and the micro-canonical statistical multi-fragmentation model is used to describe the disintegration of highly excited fragments of nuclear reactions.

Interpretation of neutron spectra have the advantage of being independent of the Coulomb barrier in the exit channel, moreover neutron emission cross sections are generally much larger than those for charged particle emission. However the experimental measurement of neutron spectra could be more challenging, requiring careful consideration of background, scattering from surrounding materials, good beam collimation, cross talk between detectors and uncertainties arising from detector efficiency considerations.

In recent years a few measurements of neutron multiplicities were carried out using ^{16,18}O and ^{19}F as projectiles on some isotopes of Pt to study the shell closure effects [16 – 19]. Also, Ramachandran et al., [20] have measured neutron, proton and α particles multiplicities for ^{28}Si+^{175}Lu. Very recently, Manoj Kumar Sharma et al. [21] have made experimental measurements with ^{12}C and ^{16}O on a few heavy targets. The motivation of our work is to look at the global prediction of pre-equilibrium and breakup effects without specific reference to level density enhancement near magic numbers.

In the present work we have measured ^{19}F induced neutron spectra for three targets ^{51}V, ^{89}Y, ^{181}Ta spanning a wide mass range and four beam energies (130, 140, 145 and 150 MeV). The measurement was carried out over 8 laboratory angles (25$^{\rm o}$, 42$^{\rm o}$, 58$^{\rm o}$, 74$^{\rm o}$, 95$^{\rm o}$, 111$^{\rm o}$, 127$^{\rm o}$ and 143$^{\rm o}$) spanning a wide angular range. Experimental details are given in Section II. Sections III and IV give brief details about the ALICE2014 and PACE4 calculations and presents a comparison of the calculations with the experimental results. A number of interesting points arise from the comparison and these are discussed in Section V.

II. Experimental details

In the present experiment, a pulsed ^{19}F beam obtained from the Bhabha Atomic Research Centre-Tata Institute of Fundamental Research (BARC-TIFR) Pelletron-LINAC

facility, Mumbai have been utilized. The pulsed beam had a two-bunch structure with a time of 106.67 ns between bunches. Beam current are in the range of 1-3 pnA were used. All the targets were rolled from spectroscopic grade material to the thicknesses in the range of 1.5-1.8 mg/cm^2. Target thicknesses were determined by accurate weighing with a micro-balance. Targets were checked for impurities using the X-ray fluorescence technique.

Fourteen liquid scintillator neutron detectors (NE213) were used to cover the angular range 25°-143°. The time of flight (TOF) distances were in the range of 65-82 cm. Special care was taken to reduce the background from the scattered neutrons. The beam dump, 1.5 m downstream was shielded with concrete blocks. No beam line collimators near the target were used. The beam focusing and steering were periodically checked to ensure low background from the target frame. The background estimations were done using a blank target and shadow bar technique.

LAMPS-VME (Linux Advanced Multi-Parameter System – VERSA-Module Euro card) [22] data acquisition system was used triggered by an OR condition from the individual detectors qualified by beam RF signal. For each detector, time-of-flight (TOF), pulse-shape discrimination (PSD) and anode signal amplitudes were recorded. The trigger logic ensured that the next master gate was blocked during busy of the VME modules. Dead time was deduced from scalars which counted raw master gates and blocked master gates. The detector efficiencies were obtained by making the measurements with a ^{252}Cf source on a thin (0.5 mm) stainless steel disk, kept at the target position enclosed in a small 4π ionization chamber detecting fission fragments. In this case TOF was measured with respect to fission fragments. Comparison was made with the efficiency curve of the neutron detector as a function of neutron energy obtained by using the Monte Carlo computer code (NEFF) [23]. The detector thresholds in the code were adjusted to match the experimental results. The neutron spectrum from ^{252}Cf is well known and its shape has been parameterized [24]. An overall agreement between the simulation results and the measured efficiencies was obtained (Fig 1).

The neutron energy spectra were obtained by converting TOF to energy on an event by-event basis using the LAMPS program. Normalization was done in terms of target thickness (which was carefully measured), beam charge (from a calibrated current integrator) and detector efficiencies. TOF calibration was done by matching the distance between the 2 gamma peaks to the beam bunch separation (106.67 ns). The graphical cuts were applied in the two dimensional spectrum to select the neutrons. This is a polygonal gate in the two dimensional spectrum of time-of-flight vs. pulse-shape discrimination signal used to distinguish neutrons from gamma rays. A typical two-dimensional plot of TOF vs. PSD is

given in Fig **2**. This figure shows a clear separation between neutron and gamma radiations. In the figure, the gamma rays correspond to smaller values of the TOF and the PSD signals. The measured spectra were normalized using the simulated efficiencies over the energy range 1.5 - 17 MeV.

The estimated errors in the present measurement include statistical error and systematic errors arising from estimating target thickness, integrated beam current and detector efficiency. The overall error in the present measurement were in the range of 8-10%. These errors have been shown in Figs. **3-14**. These estimated errors are smaller than the experimental scatter point size.

III. Details of ALICE2014 calculations

The ALICE2014 code principally uses Monte-Carlo simulations on Geometry Dependent Hybrid model (GDH) for pre-equilibrium calculations and Weisskopf-Ewing evaporation for equilibrium emission part.

It uses the fact that, three exciton configuration produced by the interaction of a nucleon with a nucleus in a two body process should give approximately the nucleon energy distribution represented by the 3 exciton density function. The angular distribution calculations are done using Chadwick-Oblozinsky linear momentum conservation model [**10, 11**]. In the Monte Carlo approach [**7**], each successive scattering of a nucleon is treated as producing a new 3-exciton configuration, consistent with the 2-body assumption. This avoids use of the higher order exciton densities which were inconsistent with population by a two body mechanism [**25**]. This Monte Carlo approach can be used to calculate multiplicities of pre-compound emitted nucleons. In other words, Monte Carlo approach allows more than one emission of pre-equilibrium ejectiles (so called multiple pre-equilibrium).

For nearly four decades, the geometry dependent hybrid model (GDH) proposed by M. Blann [**26**] have been used successfully for the modelling of non-equilibrium particle and light cluster emission in nuclear reactions induced by intermediate energy particles. In the GDH model the pre-equilibrium energy distribution of nucleons is calculated as follows:

$$\frac{d\sigma}{d\varepsilon_x} = \pi^2 \sum_{l=0}^{\infty} (2l+1) T_l \sum_{n=n_0} X_x^n \frac{\omega(p-1,h,U)}{\omega(p.h.E)} \frac{\lambda_x^e}{\lambda_x^e + \lambda_x^+} g D_n , \qquad (1)$$

where T_l is the transmission coefficient for l-th partial wave; X_x^n is the number of nucleons of type "x" in the n-exciton state; ε_x is the channel energy of the nucleon; $\omega(p.h.E)$ is the density of exciton states with "p" particles and "h" holes ($p + h = n$) at the excitation energy

E; U is the final excitation energy, $U = E - Q_x - \varepsilon_x$ and Q_x is the nucleon separation energy; D_n is the "depletion" factor; n_0 is the initial exciton number.

The nucleon emission rate λ_x^e is equal to: [27],

$$\lambda_x^e = \frac{(2S_x + 1)\mu_x \varepsilon_x \sigma_x^{inv}(\varepsilon_x)}{\pi^2 3 g_x},$$

where S_x and μ_x are the spin and reduced mass of the outgoing nucleon of type ''x'', σ_x^{inv} is the inverse reaction cross-section for particle ''x'', and g_x is the single-nucleon state density. The l-depend intra-nuclear transition rate λ_x^+ is calculated using the nucleon-nucleon scattering cross-section corrected for the Pauli principle and the average nuclear matter density at the distance from l to $(l + 1)$. For nucleon induced reactions the density of excited states with the number of excitons with n = 2 and 3 is obtained considering the finite depth of the nuclear potential well. The number of nucleons of x-type in the n-exciton state X_x^n is calculated using the ratio of the nucleon-nucleon cross-sections obtained by taking into account the Pauli principle and the nucleon motion. Multiple pre-compound nucleon emission is simulated by means of Monte-Carlo Simulation.

Equilibrium emission was calculated according to Weisskopf-Ewing (WE) model [28] neglecting angular momentum. In the evaporation model, the basic parameters are binding energies, inverse reaction cross-section, the pairing and the level-density parameters. The reaction cross-section for incident channel a and exit channel b can be written as:

$$\sigma_{ab}^{WE} = \sigma_{ab}(E_{inc}) \frac{\Gamma_b}{\sum_{b'} \Gamma_{b'}},$$

Where, E_{inc} is the incident energy. Γ_b is expressed as

$$\Gamma_b = \frac{2s_b + 1}{\pi^2 \hbar^2} \mu_b \int \sigma_b^{inv}(\varepsilon) \varepsilon \frac{\omega_1(U)}{\omega_1(E)} \, d\varepsilon,$$

Where U, μ_b and s_b are the excitation energies, the reduced mass and the spin, of the residual nucleus respectively. $\sigma_b^{inv}(\varepsilon)$ is the inverse reaction cross-section. $\omega_1(E)$ is the total single-particle level density which is given by

$$\omega_1(E) = \frac{1}{\sqrt{48}} \frac{\exp\left[2\sqrt{\alpha(E - D)}\right]}{E - D}, \quad \alpha = \frac{6}{\pi^2} g,$$

The calculations using this code have been done without parameter adjustment by selecting the Obninsk (OB) [29] as well as Kataria-Ramamurthy-Kapoor (KRK) level density options [30]. The OB level density option gives a better reproduction to our data as compared

to KRK level density and other options [30, 31]. A comparison of the experimental results with ALICE2014 calculations are given in Figs. 3-18.

IV. Details of PACE4 Calculation

The statistical model code Projection-Angular-Momentum-Coupled-Evaporation (PACE4) uses a Monte-Carlo procedure to determine the decay sequence of an excited nucleus using the Hauser-Feshbach formalism. Sequential decays are considered until any further decay is prohibited due to the energy and angular momentum conservation laws. A random number selection determines the actual final state to which the nucleus decays to and the process is, then repeated for other cascades until all the nuclei reach the ground state. The transmission coefficients for light particle emission (n, p, α) are determined using optical model potentials [32, 33]. The code also provides event by event trace back of the entire decay sequence from the compound nucleus into any one of the exit channels. The fusion cross-sections are obtained from the Bass model [34]. The fission probability is calculated using the Bohr-Wheeler saddle point formalism [35]. PACE4 code has ability to provide information on energy and angular distributions of evaporated particles.

The partial cross-section for CN formation at angular momentum (ℓ) and specific bombarding energy is given by,

$$\sigma_l = \frac{\pi \lambda^2}{4\pi^2}(2l + 1)T_l \,,$$

Where, λ is the reduced wavelength and T_l is the transmission coefficient given by,

$$T_l = [1 + \exp(l - l_{max})/\delta]^{-1}$$

Where δ is the diffuseness parameter and l_{max} is determined by the total fusion cross-section σ_F, and

$$\sigma_F = \sum_{l=0}^{\infty} \sigma_l$$

A comparison of the experimental results with the PACE4 calculations (dashed lines) are given in Figs. 3-18.

V. Discussion and Conclusions

A comparison of the results with the calculations reveal that the ALICE2014 code is fairly successful in predicting the angle-dependent spectra globally for all the targets without any parameter adjustment. We have used both OB and KRK level density in our calculations. Results using the KRK level density were somewhat inferior. In another work [6] we have also concluded that the OB level density with ALICE2014 model works well, while the results with KRK level density are not as good. The PACE4 calculations were done with the Fermi gas level density using the level density parameter a=A/10 MeV^{-1}.

Figs **3-14** (angle-dependent energy spectra), Figs **15-17** (energy-dependent angular distributions at 150 MeV beam energy) and Fig **18** (energy integrated angular distribution at 150 MeV beam energy) show a comparison of calculated results with the measured data. The ALICE2014 code is fairly successful in reproducing the results globally without any parameter adjustment. The OB level density was found to give better results than the KRK level density. This was also the case in an earlier work [6].

PACE4 calculations were done with the Fermi gas level density using the level density parameter a=A/10 MeV^{-1}. The low neutron energy region (below approximately 8 MeV), is dominated by statistical evaporation, while at higher neutron energies, the contribution of pre-equilibrium emission and breakup and related processes are expected to be large, especially at highest beam energy. At low energies also there may be a contribution of the breakup reaction which is not included in PACE4. In ALICE2014 breakup is included in an approximate way [13, 15]. Both contributions are forward peaked, however pre-equilibrium emission increases for higher neutron energies. Considering the overall picture first, Fig. **18,** plotted only at the highest beam energy, clearly shows the forward peaked nature of the data, fairly well reproduced by ALICE2014. The PACE4 calculations tend to merge with ALICEE2014 for angles greater than 100°.

More details can be seen from the angle dependent energy spectra. Considering the spectra at the most forward angles, PACE4 calculations are lower than ALICE2014 calculations at higher neutron emission energies. The difference is greater for higher projectile energies and is more for ^{181}Ta as compared to ^{89}Y and ^{51}V. The experimental trend is in favor of ALICE2014 calculations for ^{181}Ta target, however for ^{89}Y and ^{51}V targets the data for high neutron energies, falls in-between the ALICE2014 and PACE4 predictions. Similarly, at the most forward angles and at the lowest neutron energies, PACE4 predictions are underestimated as compared to the data, while ALICE2014 predictions approximately reproduce the data. At these forward angles the breakup contribution is expected to be high. At intermediate angles around 90°-100°, ALICE2014 and PACE4 calculations are fairly close

for all the targets and the experimental measurements are well predicted by both calculations. Here the contribution from breakup and pre-equilibrium are supposed to be small.

It is interesting to examine the spectra at 25°. In all the cases, it is observed that there is a fall in the PACE4 calculations at low (below 2 MeV) as well as at high energies. The effect is most pronounced at the highest beam energy. Deviations at lower neutron energy may be due to breakup or other reaction mechanism such as transfer and this is expected to be higher for heavier target. At high neutron energy the pre-equilibrium effect may also become important as evident from the reasonably good agreement shown by the ALICE2014 predictions. Pre-equilibrium emission is expected to be more in the heavy mass target (^{181}Ta) as compared to the light and medium mass targets (^{51}V and ^{89}Y) and increases with beam energy. Breakup is expected to be higher for heavier target, however, the fall of PACE4 cross sections at 25° for the lowest neutron energies are stronger for lighter target, being strongest for the ^{51}V target where a fall can also be observed around the region of 42°, indicating that breakup or something other than breakup might also be playing a role.

At the most backward angle at high emission energies, the reproduction of data for ^{181}Ta target is not as good. Considering the ^{181}Ta target, at beam energy 130 MeV, the PACE4 calculation falls off faster than the ALICE2014 calculation, but the experimental data is somewhat higher than the ALICE2014 prediction. At beam energy 150 MeV, the two calculations are similar in trend, but the measured data is higher. Considering the ^{89}Y target, the data are in agreement with ALICE2014 but the PACE4 calculations fall off only slightly faster. In the case of the ^{51}V target, the data clearly favor the ALICE2014 calculations which are substantially higher than the PACE4 calculations at higher neutron energies. Thus, it appears that there may be pre-equilibrium effects which cause more neutron emission at higher energies, even at 143°. This is not predicted by the ALICE2014 calculation for the heaviest target, but is correctly predicted for the lightest target.

The above observations can be further clarified from angular distribution plots for ^{19}F + ^{181}Ta, ^{89}Y, ^{51}V systems at the highest beam energy of 150 MeV, (Figs. **15-17**). In the case of heavy (^{181}Ta) system (Fig. **15**), there is considerable amount of pre-equilibrium neutron emission at higher neutron energies as expected in the heavy targets. However, in this system, the ALICE2014 calculations slightly under predict the data. At the lowest neutron energies, ALICE2014 also under predicts the experimental results. It can be clearly observed that for the medium (^{89}Y) (Fig. **16**) and the light (^{51}V) (Fig. **17**) systems with the increase of emitted neutron energies, there is a considerable gap between the PACE4 and ALICE2014 results at forward angles below 50^{0}. PACE4 calculations grossly underestimate the experimental

results in this region. The close agreement between experimental results and ALICE2014 prediction at all the neutron energies, may be an indication of breakup and/or pre-equilibrium emission. At backward angles, above 50^0, both PACE4 and ALICE2014 reproduce the experimental results, thereby indicating absence of pre-equilibrium and breakup. At most backward angles at high emission energies, the reproduction of data is not as good for ^{181}Ta target. In Fig. 18 the failure of ALICE2014 for ^{181}Ta target at 25° is worth attention. This could be a short coming of the simplified breakup model used in the ALICE2014 predictions [15]. This figure also brings out the dependence of combined breakup and pre-equilibrium effect as a function of target mass.

In summary, we have made an experimental measurement of neutron spectra in ^{19}F induced reactions for three targets. The trend of the data is well reproduced by ALICE2014 calculations. A comparison with PACE4 calculations which includes only statistical evaporation brings out the contributions arising from breakup and pre-equilibrium effects. Both arise at forward angles, however the former contributes to the low-energy part of the spectra, while the latter contributes at higher neutron energies. While calculations using the ALICE2014 model with OB level densities reproduce the data globally quite well, a few short comings have been pointed out. It may be remarked cautiously that the breakup comes at lower neutron energies and forward angles while pre-equilibrium comes at high neutron energies and forward angles. PACE does not include breakup. In our graphs it is seen in the low-energy part of the spectra that PACE underestimates while ALICE2014 does better. This may be because the breakup of light particle is included in the ALICE2014 code. From the present study it may also be concluded that the target mass dependence on the reaction mechanism cannot be ignored. Some shortcomings of the ALICE2014 calculations are also brought out.

Acknowledgements

References

[1] M. Blann, Ann. Rev. Nucl. Sci. 25, 123 (1975).

[2] Griffin, J.J. Phys. Rev. Lett. 17, 478 (1976); Phys. Lett. 24B, 5 (1967).

[3] E. Gadioli, Erba E. Gadioli, Erba, J.J. Hogan, and K.I. Burns, Z. Phys. A301, 289 (1981).

[4] H. Feshbach, A. Kerman and S. Koonin, Ann. Phys. 125, 429 (1980).

[5] R. Bonetti, L. Colli-Milazzo, M. Camnasio, P.E. Hodgson, Phys. Rev. C24, 71 (1981).

[6] J. Acharya, S. Mukherjee, G. F. Steyn, N. L. Singh, and A. Chatterjee, Phys. Rev. C 93, 024608 (2016)

[7] M. Blann, Phys. Rev. C **54**, 1341 (1996)

[8] M. Blann and M. B. Chadwick, Phys. Rev. C **57**, 233 (1998).

[9] M. Blann and M. B. Chadwick, Phys. Rev. C **62**, 034604 (2000).

[10] M. B. Chadwick and P. Oblozinsky, Phys. Rev. C 46, 2028 (1992).

[11] M. B. Chadwick and P. Oblozinsky, Phys. Rev. C 50, 2490 (1994).

[12] L. Brito and B.V. Carlson, EPJ Web of Conferences **69**, 00024 (2014).

[13] M. Blann and A. Y. Konobeev, Pre-compound Cluster Decay in HMSALICE (2008) (unpublished), available in documentation supplied with RSICC code package PSR-550 (Package name – ALICE 2014/ALICE 2017), https://rsicc.ornl.gov /codes /psr/psr5/psr-550.html

[14] A. Gavron, Phys. Rev. C21, 230 (1980).

[15] B.V. Carlson et al., Journal of Physics: Conference Series 312, 082017 (2011).

[16] Varinderjit Singh et al., Phys. Rev. C **87**, 064601 (2013).

[17] Rohit Sandal et al., Phys. Rev. C **87**, 014604 (2013).

[18] Varinderjit Singh et al., Phys. Rev. C **86**, 014609 (2012).

[19] F. Gramegna et al., Journal of Physics: Conference Series, 580, 012011 (2015).

[20] K. Ramachandran et al., Phys. Rev. C **73**, 064609 (2006).

[21] Manoj Kumar Sharma et al., Phys. Rev. C **91**, 014603 (2015).

[22] http://www.tifr.res.in/~pell/lamps.html

[23] G. Dietze and H. Klein, NRESP4 and NEFF4 Monte Carlo Code for the Calculation of Neutron Response Functions and Detection Efficiencies for NE213 Scintillation Detectors. PTB-ND-22. Physikalisch-Technische Bundesanstalt, Braunschweig, Germany. (1982)

[24] D. G. Madland and J. R. Nix, in *Proceedings of the Conference on Nuclear Data for Science and Technology*, edited by K.H. Bockhoff (Antwerp, Belgium, 1983), p. 473.

[25] J. Bisplinghoff, Phys. Rev. C 33, 1569 (1986).

[26] M. Blann, Phys. Rev. Lett. 28, 757 (1972).

[27] M. Avrigeanu and V. Avrigeanu, IAEA0971, NEA Data Bank (1996).

[28] V.F. Weisskopf and D.H. Ewing, Phys. Rev. 57, 472 (1940).

[29] A. V. Ignatyuk, J. L. Weil, S. Raman, and S. Kahane, Phys. Rev. C 47, 1504 (1993).

[30] S. K. Kataria, V. S. Ramamurthy, and S. S. Kapoor, Phys. Rev. C 18, 549 (1978); Erratum Phys. Rev. C 19, 297 (1979).

[31] A. Gilbert and A.G.W. Cameron, *Can. J. Phys.*, 43, 1446 (1965).

[32] C. M. Perey and F. G. Perey; At. Nucl. Data Tables 17, 1 (1976).

[33] J. R. Huizenga and G. Igo, Nucl. Phys. 29, 462 (1962).

[34] R. Bass, Phys. Rev. Lett. 39, 265 (1977).

[35] N. Bohr and J. A. Wheeler; Phys. Rev. 56, 426 (1939).
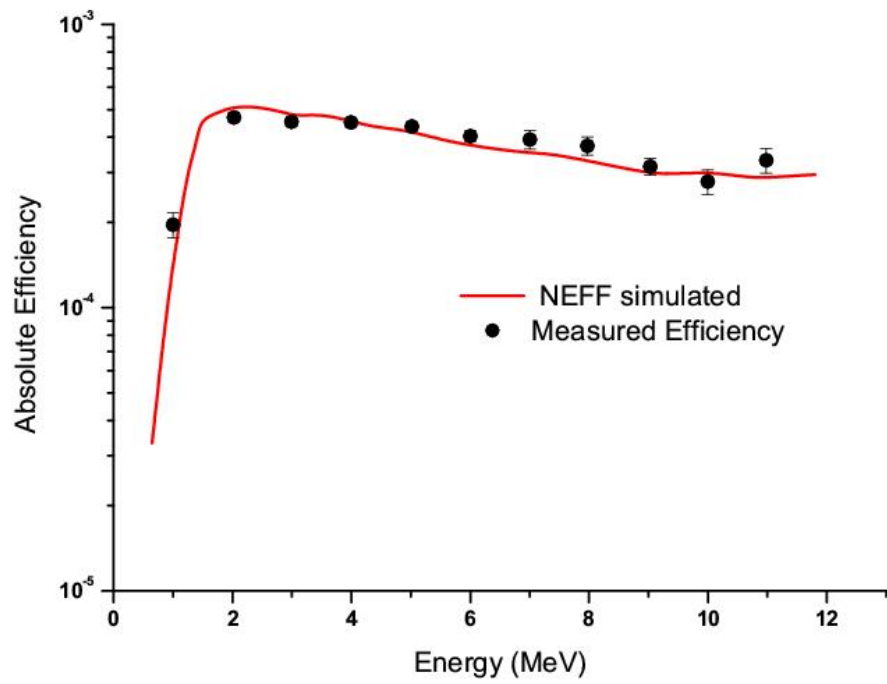
Fig 1. (Color online) Comparison of the experimentally obtained neutron efficiency (filled circles) with the same obtained using Monte Carlo simulation code NEFF (solid line).
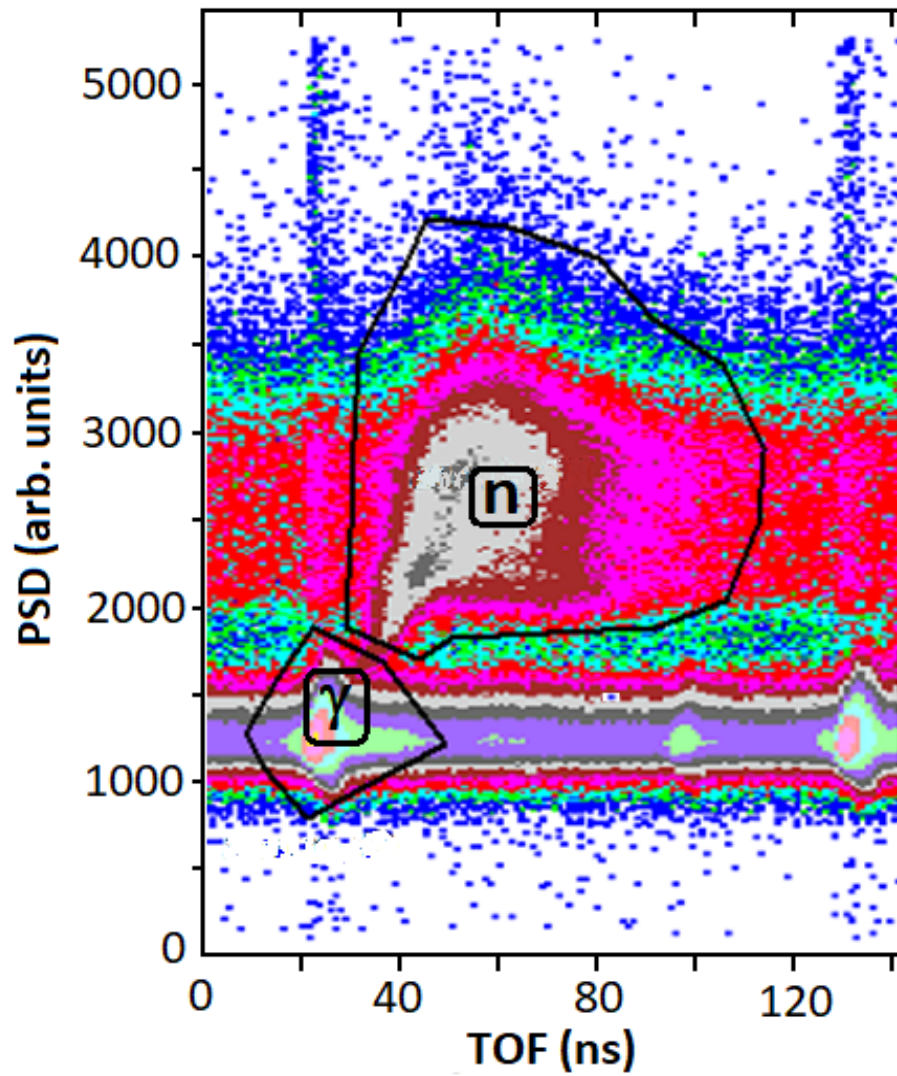
**Fig 2. (Color online)** Typical plot of pulse shape discrimination (PSD) signal versus time-of-flight (TOF) signal.
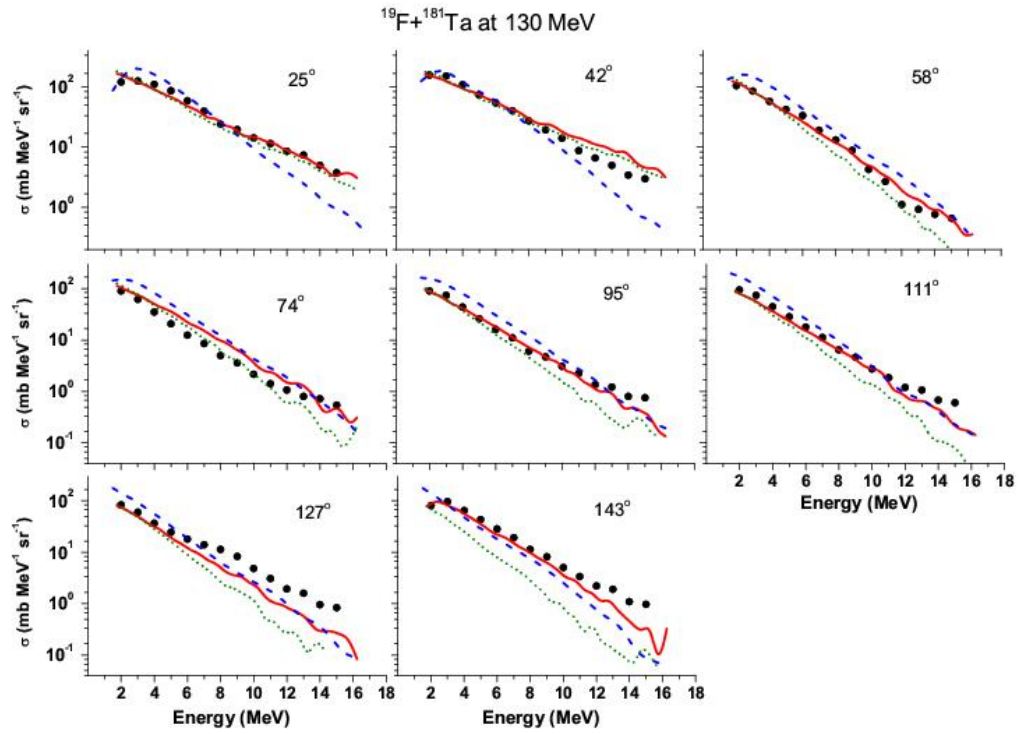
Fig 3. (Color online) Neutron emission differential cross sections for 130 MeV ^{19}F on ^{181}Ta target. The solid symbols are the experimental results of this work. The calculated cross sections are shown as red solid curve (OB level density) and green dash-dot curve (KRK level density) as obtained with the nuclear reaction code ALICE 2014 and blue dash curve as obtained from PACE4. The estimated errors are smaller than the experimental scatter point size.
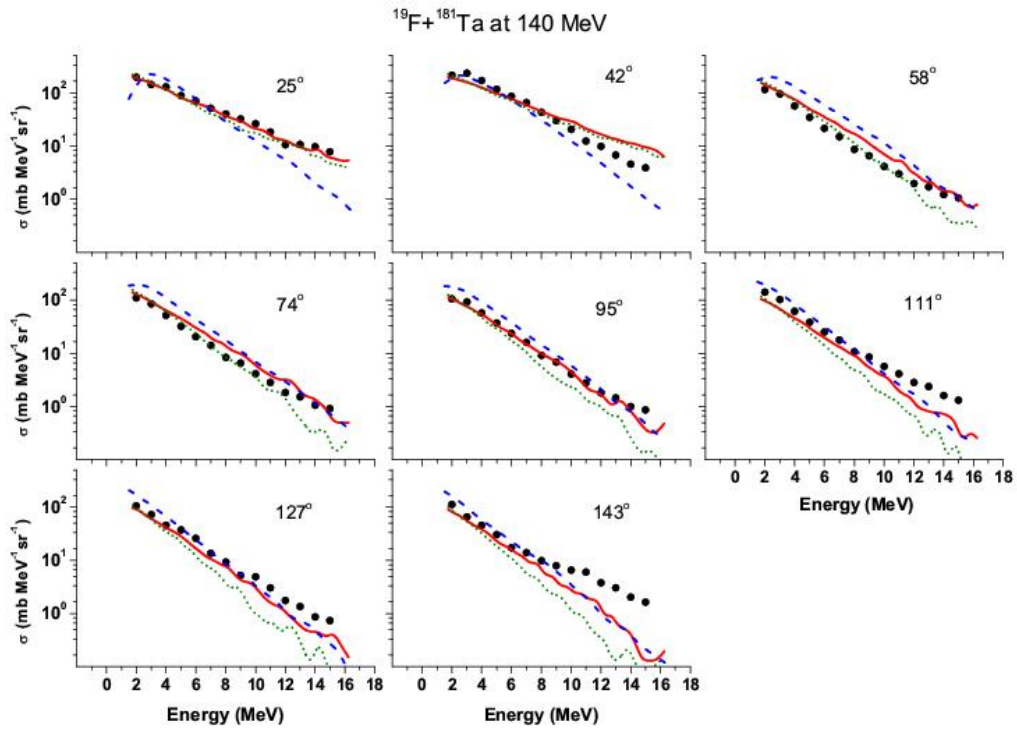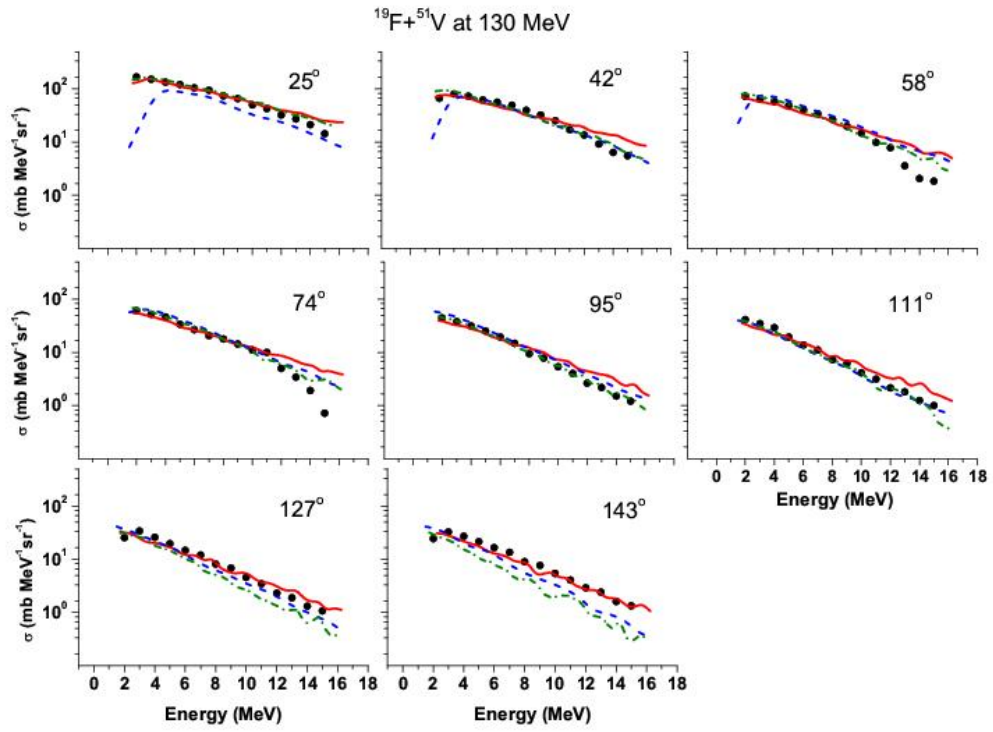
Fig 4. (Color online) Neutron emission differential cross sections for 140 MeV ^{19}F on ^{181}Ta target. The other details are same as in Fig. 3.
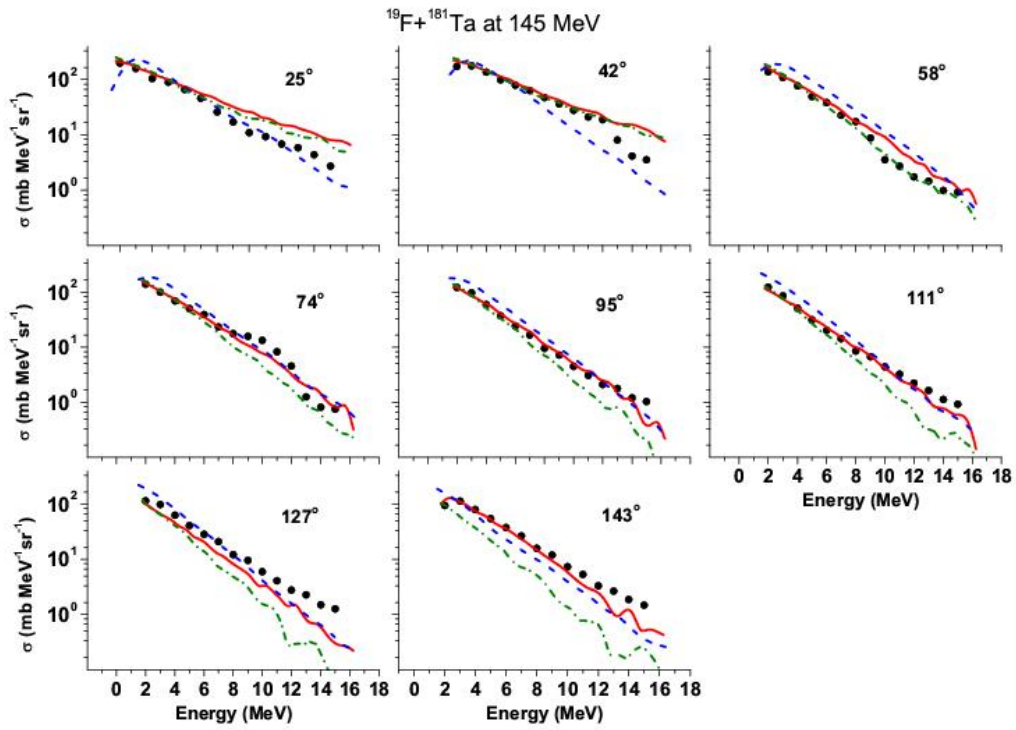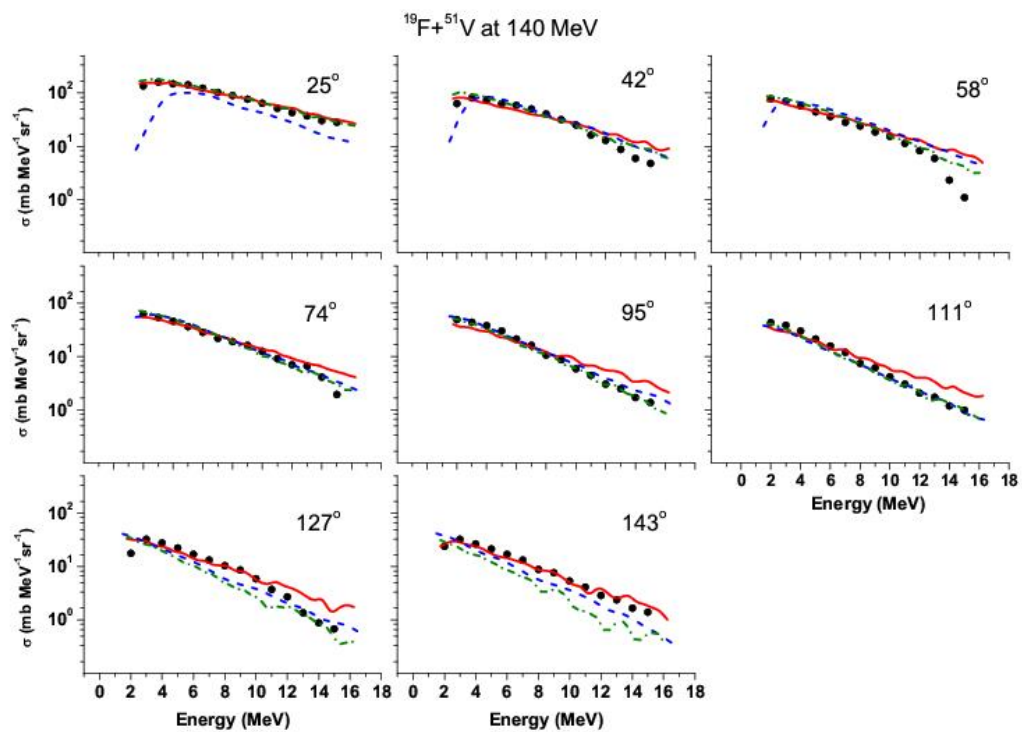
Fig 5. (Color online) Neutron emission differential cross sections for 145 MeV ^{19}F on ^{181}Ta target. The other details are same as in Fig. 3.
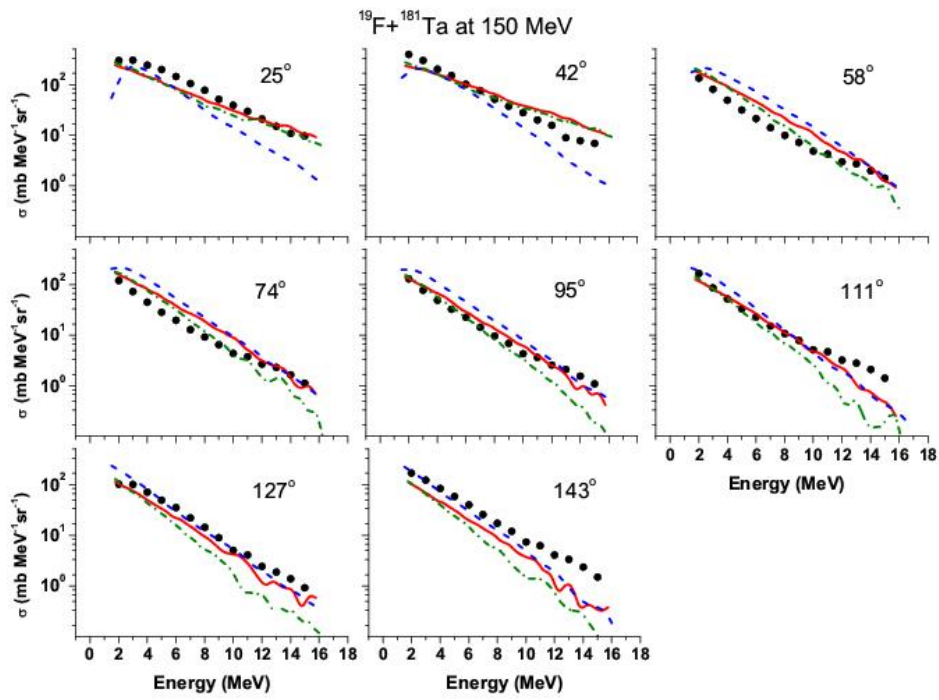
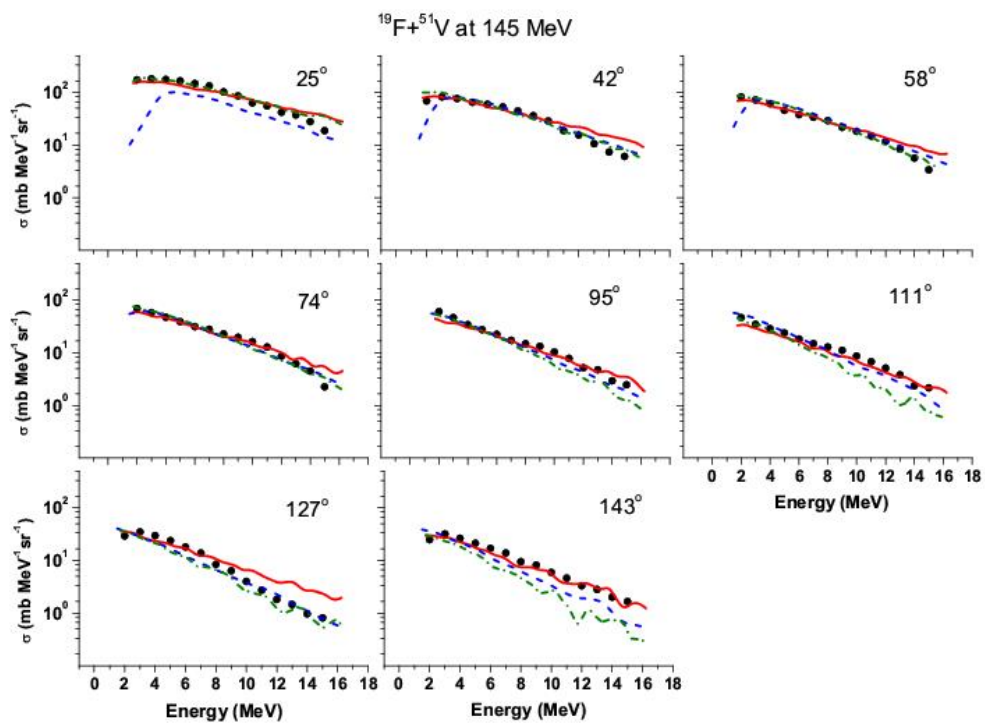**Fig 6. (Color online)** Neutron emission differential cross sections for 150 MeV ^{19}F on ^{181}Ta target. The other details are same as in Fig. 3.
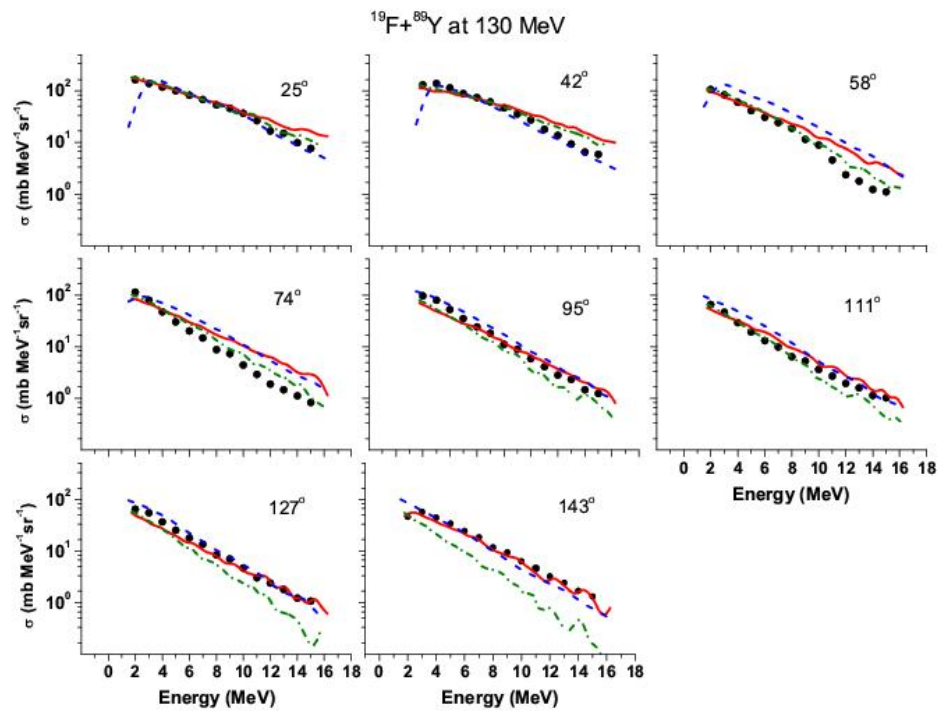
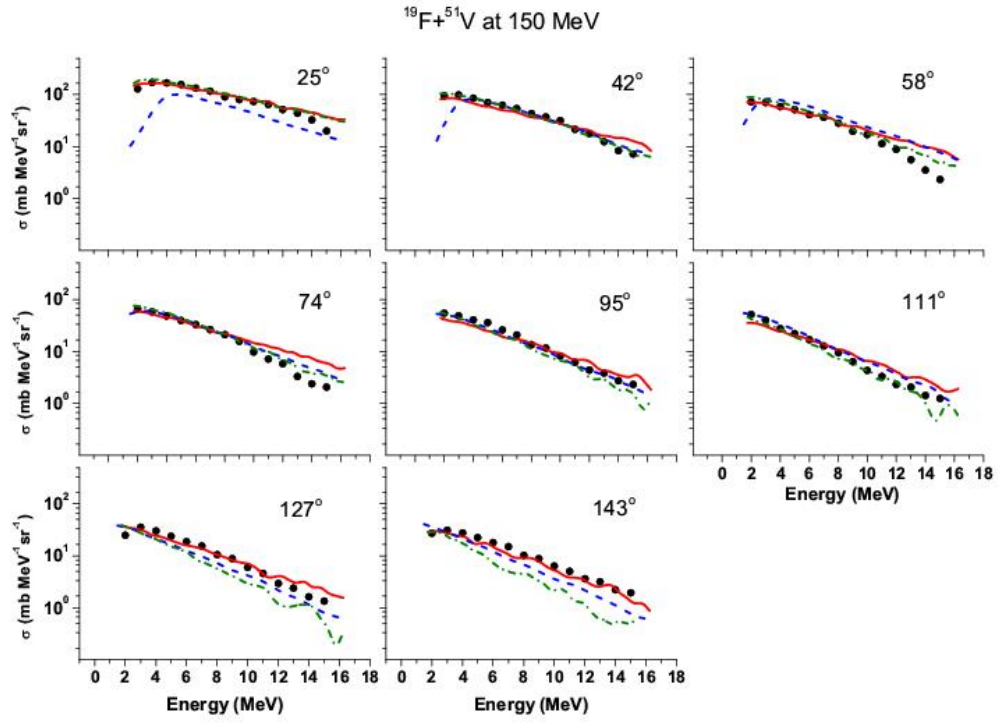**Fig 7. (Color online)** Neutron emission differential cross sections for 130 MeV ^{19}F on [89]Y target. The other details are same as in Fig. 3.
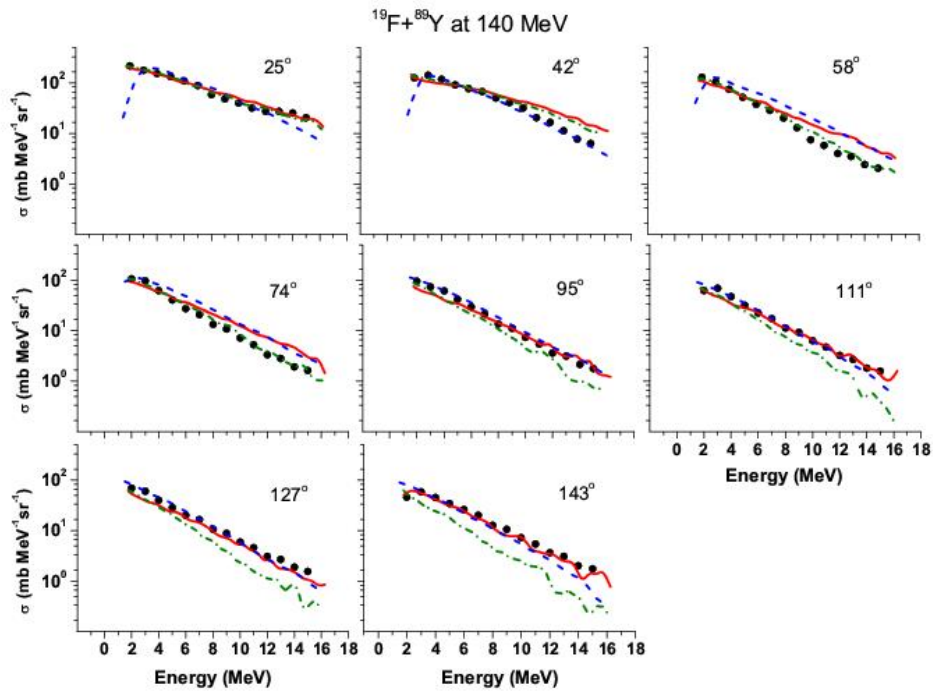
Fig 8. (Color online) Neutron emission differential cross sections for 140 MeV ^{19}F on ^{89}Y target. The other details are same as in Fig. 3.
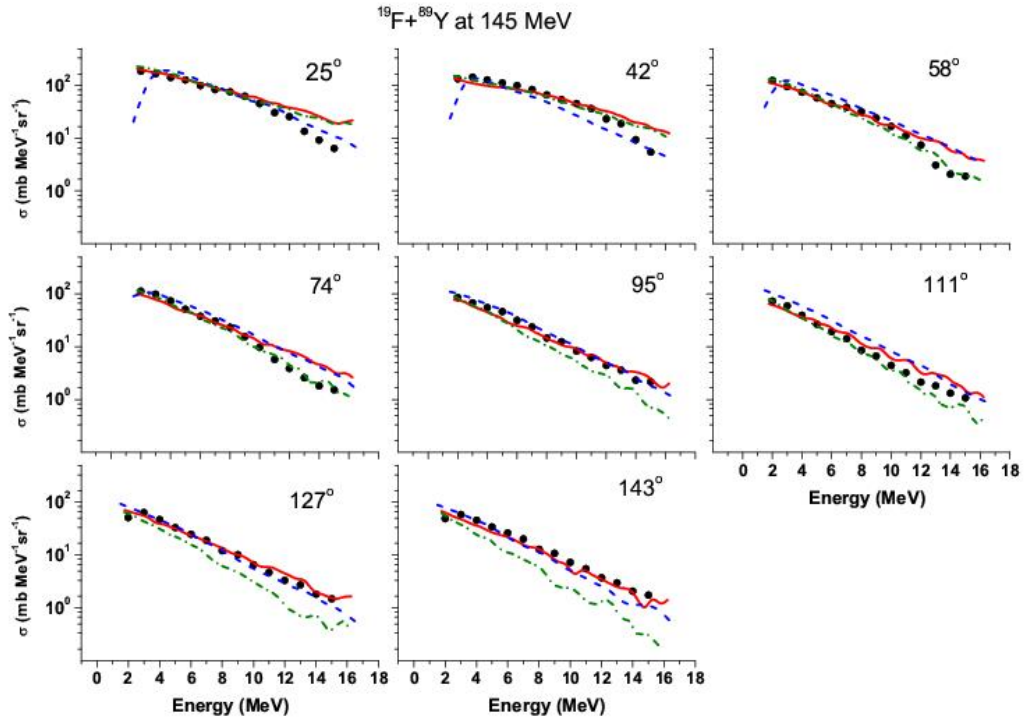
Fig 9. (Color online) Neutron emission differential cross sections for 145 MeV ^{19}F on ^{89}Y target. The other details are same as in Fig. 3.
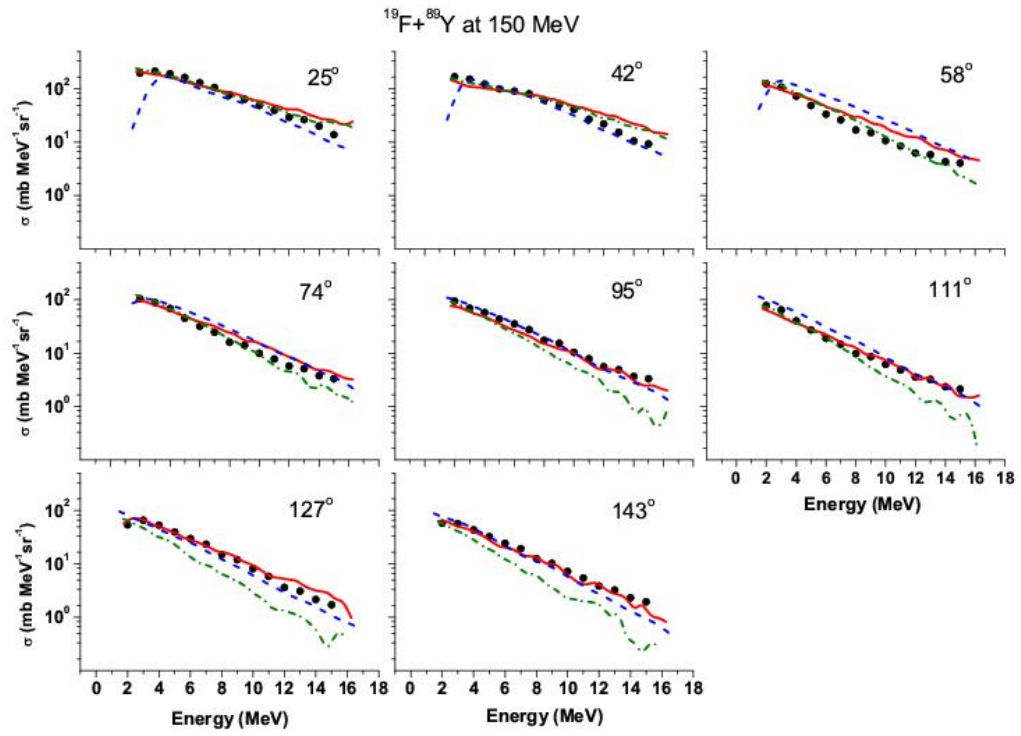
**Fig 10. (Color online)** Neutron emission differential cross sections for 150 MeV ^{19}F on ^{89}Y target. The other details are same as in Fig. 3.

Fig 11. (Color online) Neutron emission differential cross sections for 130 MeV ^{19}F on ^{51}V target. The other details are same as in Fig. 3.

**Fig 12. (Color online)** Neutron emission differential cross sections for 140 MeV ^{19}F on ^{51}V target. The other details are same as in Fig. 3.

Fig 13. (Color online) Neutron emission differential cross sections for 145 MeV ^{19}F on ^{51}V target. The other details are same as in Fig. 3.

**Fig 14. (Color online)** Neutron emission differential cross sections for 150 MeV ^{19}F on ^{51}V target. The other details are same as in Fig. 3.
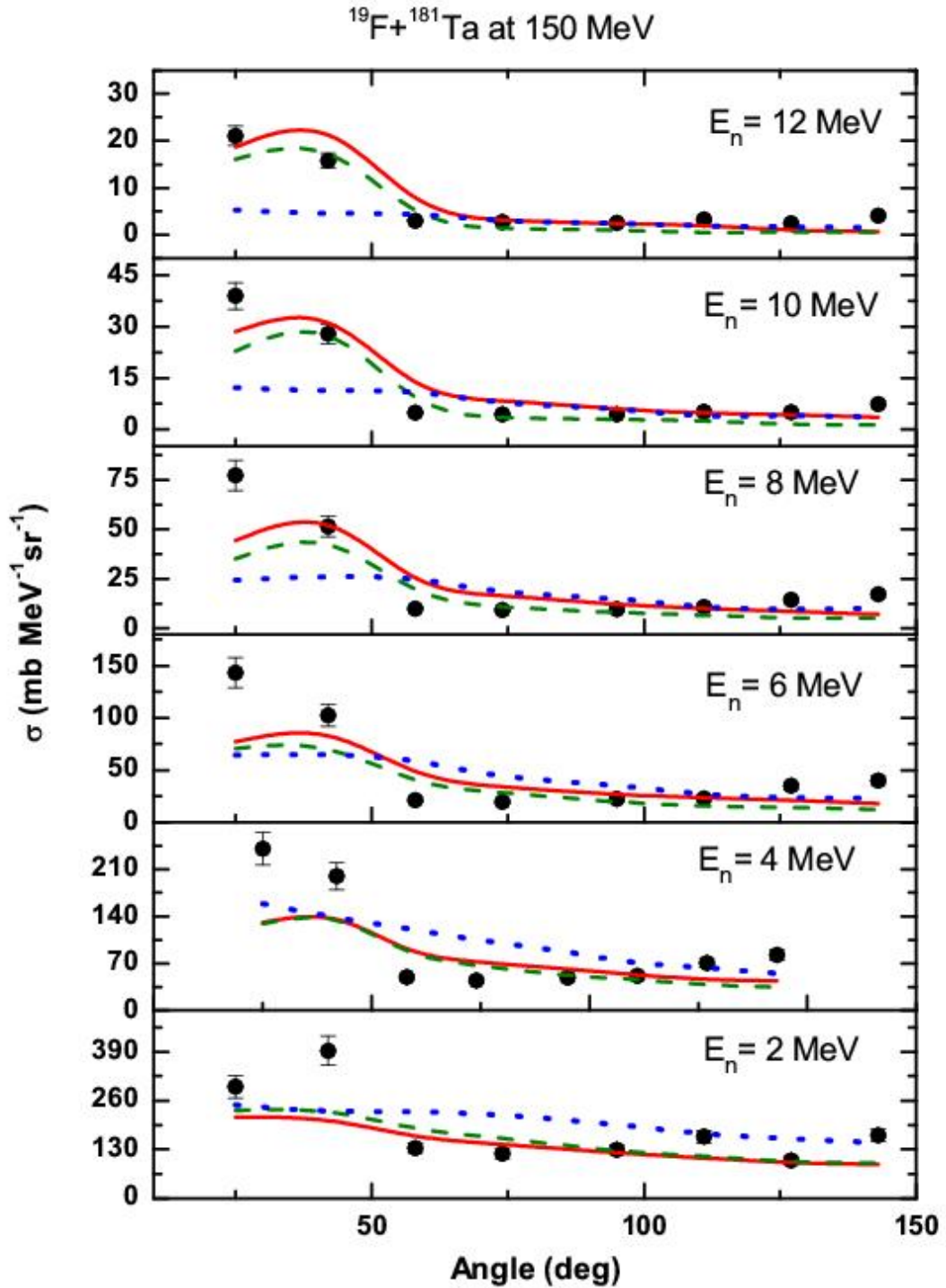
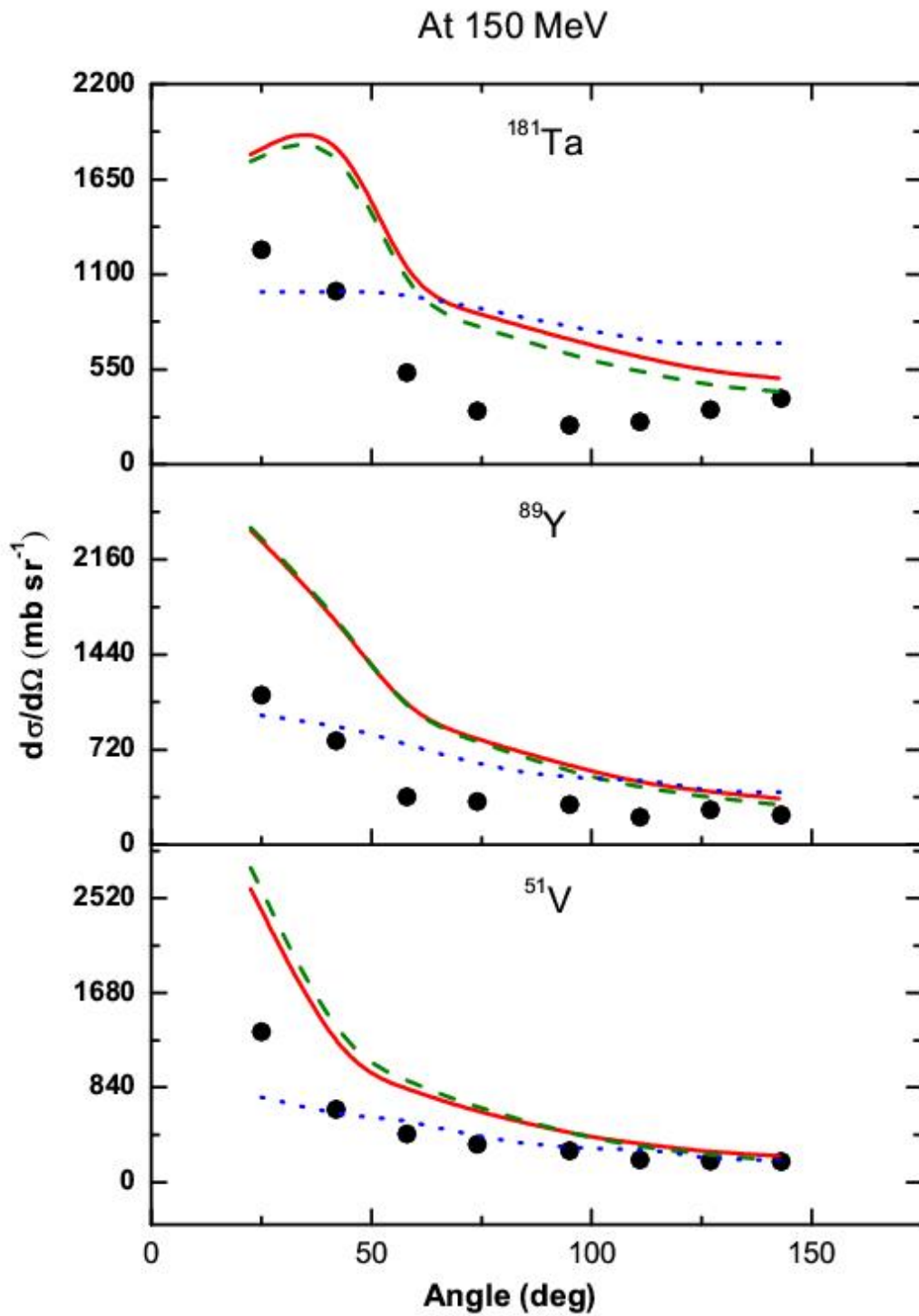**Fig 15. (Color online)** Neutron angular distribution at various emission energies for ^{19}F (150 MeV) + ^{181}Ta. PACE4 (Blue dotted curve), ALICE2014 (KRK) (Green dash curve), ALICE2014 (OB) (Red solid curve) and present experimental results (Black solid points with error bars).
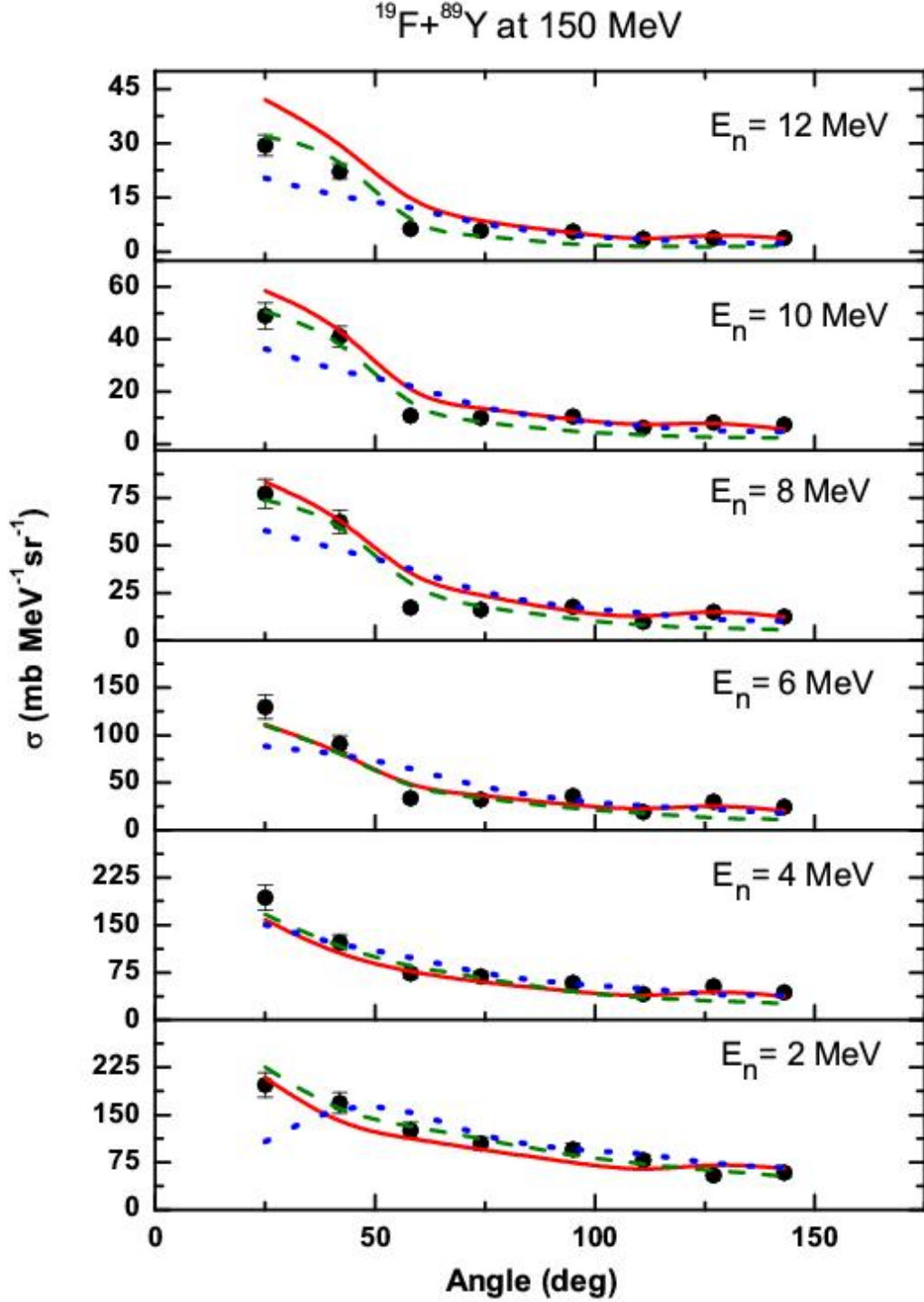
Fig 16. (Color online) Neutron angular distribution at various emission energies for ^{19}F (150 MeV) + ^{89}Y. The other details are same as in Fig. 15.
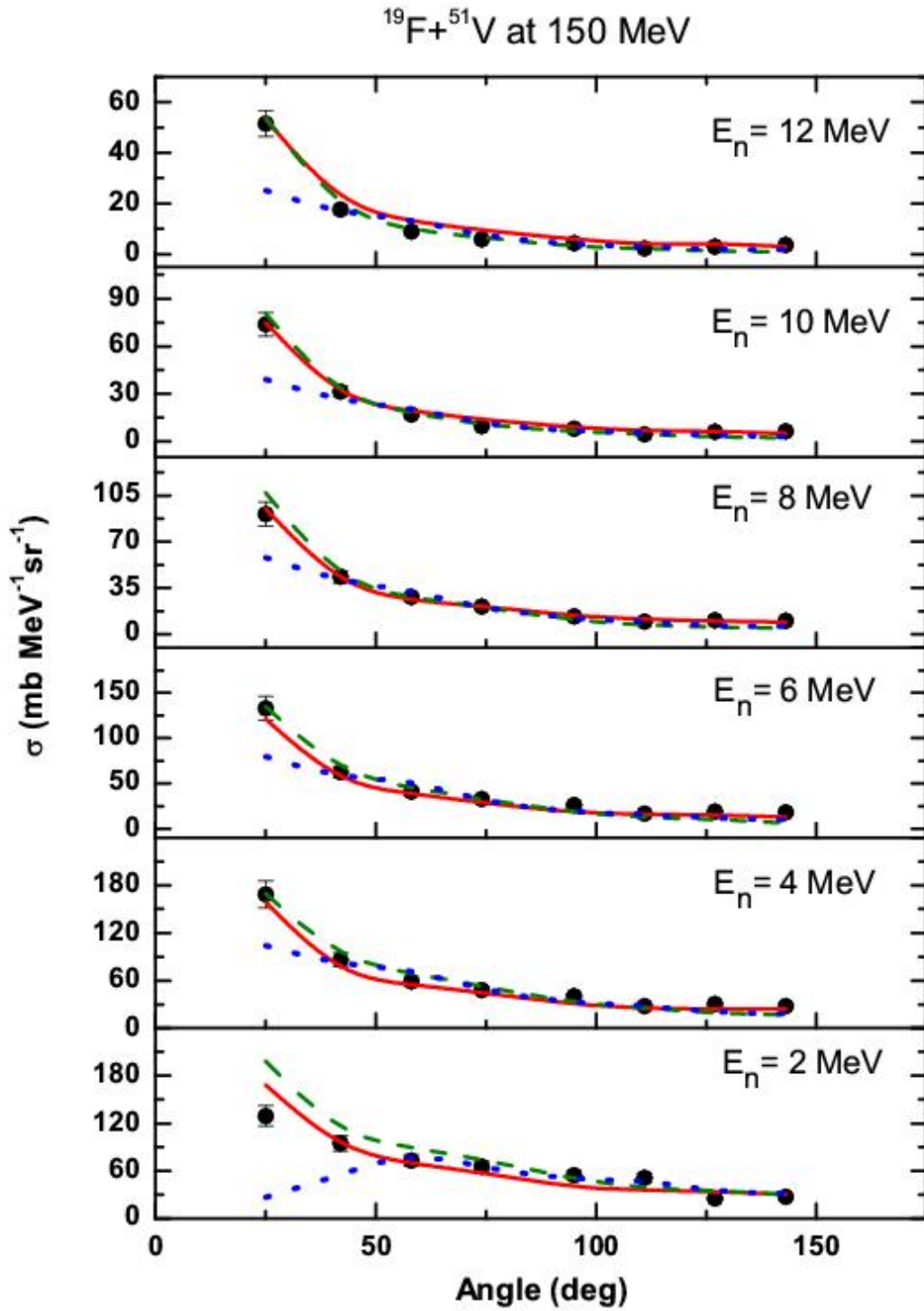
Fig 17. (Color online) Neutron angular distribution at various emission energies for ^{19}F (150 MeV) + ^{51}V. The other details are same as in Fig. 15.

Fig 18. (Color online) The energy integrated angular distribution for emitted neutrons for various targets at 150 MeV beam energy. The other details are same as in Fig.15.